2014 5th IEEE RAS & EMBS International Conference on
Biomedical Robotics and Biomechatronics (BioRob)
August 12-15, 2014. São Paulo, Brazil

Control Scheme with Tissue Interaction Detection for a Single Port Access Surgery Robotic Platform

Pérez-del-Pulgar C.J., Muñoz V.F., *Member, IEEE*

Abstract—**This paper proposes a control scheme for handling surgical instruments by a single port access surgery robotic platform. This scheme is based on a Hidden Markov Model for detecting interaction with tissue inside the abdomen and a Kalman filter measurement fusion method for estimating the fulcrum point using forces and torques exerted on several instruments. In order to perform movements taking into account the estimated fulcrum point, a parallel force-position control algorithm is proposed in order to minimize exerted forces in the patient's abdomen. At last, proposed control scheme has been implemented in a surgical robotics platform composed by two manipulators and experimental results are shown in order to demonstrate how it works.**

I. INTRODUCTION

Use of Minimally Invasive Robotics Surgery (MIRS) is totally extended in laparoscopic surgery, indeed, more than 300.000 surgical operations using a robotic system had been performed until 2010 [1]. However, most of the surgical robotics researching activities are nowadays moving forward Single Port Access Surgery (SPAS) [2]. This method uses only one incision point (fulcrum point) where the endoscopic camera and all the instruments are introduced using a multiport trocar. The advantages provided by this method compare to classic laparoscopic surgery include: fewer incisions, one instead of at least three, better cosmetic results, the scar is hidden because the incision is done in the umbilicus, and at last, minor postoperative pain and hospital stay [3][4]. On the other hand, this approach requires a better ability for surgeons, hence more training time, and an increment of the operating room time. These issues arise because the instruments are inserted by the same trocar and they both could collide within and outside the abdomen "sword fighting". Also, an inadequate triangulation between them and a reduction of the field of view appear due to obstruction by instruments [5]. To solve these issues, many robotics platforms for SPAS have been developed. They could be classified into two types: flexible robotics endoscopes with cameras and instruments [6][7][8], and surgical robotics platforms composed by manipulators which handle a laparoscopic camera and instruments [9][10]. Second type introduces several instruments through a fulcrum point which represents a constraint for the movement because manipulators have to move these instruments around it without exerting undesirable forces on the patient's abdomen. Nevertheless, this constraint has been solved using different methods: The da Vinci and other surgical platforms use a dedicated kinematic design based on a mechanical remote center of motion (RCM) which is matched with the fulcrum point [11], and it is assumed that this point is invariant during the surgery. The main advantages which provide this design is the rigidity and safety, a controller fault would not cause any damage to the patient. This is the reasons because this method is mainly used in clinical applications. For the case of generic kinematic designs, a virtual or software RCM is frequently used. This solution also provides many advantages such as changeable pivot position and increased maneuverability. In this case, location of the fulcrum point is usually estimated online during the surgery. For this purpose, several contributions have been done: Michelin et al. [12] propose a control algorithm based on the joint torques which performs movements taking into account the fulcrum point. This contribution shows several simulations which validate this algorithm. On the other hand, Krupa et al. [13] use a hybrid force-position control algorithm which uses a Force/Torque (F/T) sensor placed between the end effector of the manipulator and the instrument, performing movements around the fulcrum point. This algorithm was successfully implemented in a 6 DoF manipulator. Mentioned algorithms have been recently used in different contributions related to force feedback and haptic devices [14][15]. However, it is worth mentioning that these contributions do not take into account interaction of the instrument tip with tissue inside the abdomen. This issue could provide errors on the estimation and thus an incorrect movement of the instrument. Furthermore, it is needed to improve the fulcrum point estimation in order to minimize exerted forces on the patient's abdomen which is very useful for providing force feedback to the surgeon using these F/T sensors.

Contribution of this paper is a control scheme for handling surgical instruments by several manipulators for SPAS taking into account interaction with tissue and estimating the fulcrum point. The method for detecting interaction with tissue is based on a Hidden Markov Model and the fulcrum point estimator is based on a Kalman filter measurement fusion algorithm. These methods use information provided by two F/T sensors placed between the end effector and instrument of each manipulator. Also, proposed control scheme is based on a parallel force-position control algorithm which minimizes exerted forces in the patient's abdomen. In Section II a geometrical model of an SPAS scenario and the abdominal and tissue interaction model are described. In Section III the interaction with tissue detection method is proposed. Section IV describes the control scheme using the fulcrum point estimator and the tissue interaction detector. Finally, Section V shows the experimental results.

*This work was supported in part by the Spanish National project DPI2010-21126 and the Andalucian Regional one P07-TEP-02897.

Prof. V. F. Muñoz and C.J. Perez-del-Pulgar are with the System Engineering and Automation Department, Universidad de Málaga, Andalucia Tech, Spain (phone: +34 951 95 23 24; fax: +34 951 95 25 40; e-mail: carlosperez@uma.es).

II. Problem Statement

A. Geometrical Model

Fig. 1 shows the geometric model used to represent movements of instruments introduced by a multiport trocar for SPAS and operated by two manipulators. Fig. 1.b represents locations where $\{B_0\}$ is the base of manipulators platform, $\{B_1\}$ and $\{B_2\}$ are the base of each manipulators, $\{H_1\}$ and $\{H_2\}$ are the end effectors which are holding the surgical instrument, $\{F\}$ is the fulcrum point location for both manipulators, and $\{P_1\}$ and $\{P_2\}$ are the tip location. It is worth representing this relation by a kinematic model graph which is shown in Fig. 1.a. In this figure, ${}^{B}T_{H}$ is the homogenous transformation matrix represented by the direct kinematic model for each manipulator, ${}^{H}T_{F}$ depends on the orientation of each end effector and the distance between this one and the fulcrum point ${}^{H}D_{F}$, and at last ${}^{F}T_{P}$ depends on the distance between the fulcrum point and the tip. Furthermore, $\{F_1\}$ and $\{F_2\}$ have been defined as the estimated fulcrum point position for each manipulator and the same orientation as $\{H_1\}$ and $\{H_2\}$ respectively.

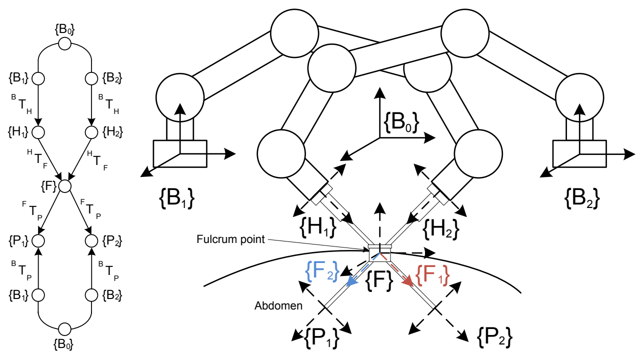

(a) (b)

Fig. 1. (a) Kinematic model graph. (b) System locations for a SPAS scenario.

In this contribution, locations are represented using a tuple with position and orientation using Euler ZYZ angles, i.e. (1), taking $\{B_0\}$ as the Cartesian coordinates origin. Also, it can be translated to a homogeneous transformation matrix ${}^{B_0}T_{A}$ where $\{A\}$ is the location.

$$\{A\} = (x_A^{B_0}, y_A^{B_0}, z_A^{B_0}, \varphi_A^{B_0}, \upsilon_A^{B_0}, \psi_A^{B_0}) \tag{1}$$

B. Abdominal and Tissue Interaction Model

Because the fulcrum point $\{F\}$ is not attached to any element of the manipulator, it is located in the trocar which is inserted into the patient's body, for each manipulator the distance between the end effector and this point is unknown. However, it could be estimated as will be shown below. An error on this estimation provides a wrong fulcrum point location $\{F'\}$, thus if a movement around this point were carried out, undesirable forces would be exerted in the patient's abdomen. Furthermore, when instruments interact with tissue, another force arises. Fig. 2 represents the interaction of the instrument with the patient's abdomen and tissue as mentioned before. It represents a rotation of the instrument in the Y axis an angle α using the estimated fulcrum point location $\{F'\}$. This movement is represented in the XZ plane and it could be extrapolated to any other movement.

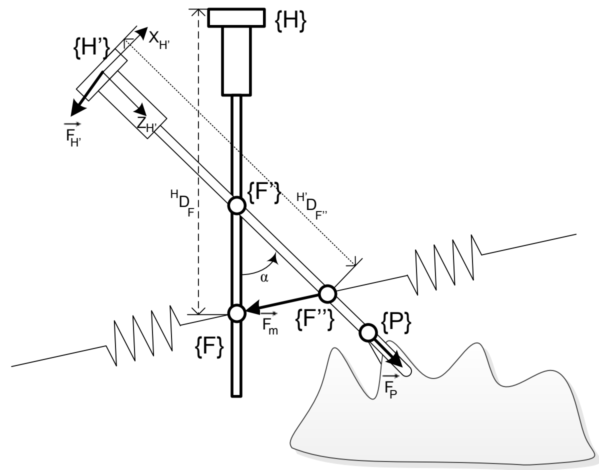

Fig. 2. Interaction with abdomen and tissue.

As shown, this movement causes a displacement from $\{F\}$ to $\{F''\}$, the distance between them is represented by $\overrightarrow{r_m}$. Assuming the abdomen as a spring based model [16], $\overrightarrow{F_m}$ represents the lateral forces exerted on the abdomen in $\{F''\}$ which is calculated by (2), where K_a is the skin elasticity constant. Moreover, when there is interaction with tissue, force $\overrightarrow{F_P}$ is exerted on the tip of the instrument. Assuming that the flexibility of the instrument is negligible, sum of $\overrightarrow{F_m}$ and $\overrightarrow{F_P}$ are transmitted to the end effector $\{H'\}$ thus $\overrightarrow{F_{H'}}$ is obtained. This force could be read by an F/T sensor placed on $\{H'\}$. Besides, because of this movement, an inertial moment $\overrightarrow{M_{H'}}$ is produced, allowing this information, using the sensor mentioned before, to estimate the distance between the end effector and the fulcrum point $\left|\overrightarrow{{}^{H'}D_{F''}}\right|$ by (3) when there is no interaction with tissue ($\overrightarrow{F_P} \approx 0$) and therefore, using (4) $\{F''\}$ is obtained.

$$\overrightarrow{F_m} = K_a \cdot \overrightarrow{r_m} \tag{2}$$

$$\overrightarrow{M_{H'}} = \overrightarrow{F_m} \cdot \overrightarrow{{}^{H'}D_{F''}} + \overrightarrow{F_P} \cdot \overrightarrow{{}^{H'}D_P} \tag{3}$$

$${}^{B}T_{F''} = {}^{B}T_{H'} \cdot \begin{bmatrix} 1 & 0 & 0 & 0 \\ 0 & 1 & 0 & 0 \\ 0 & 0 & 1 & \left|\overrightarrow{{}^{H'}D_{F''}}\right| \\ 0 & 0 & 0 & 1 \end{bmatrix} \tag{4}$$

Finally, using only $\overrightarrow{F_{H'}}$ is impossible to know if there is interaction with tissue or not. For this reason, a method for detecting this interaction is proposed in next section.

III. Interaction with Tissue Detector

As mentioned before, when there is interaction with tissue ($\overrightarrow{F_P} \neq 0$), it is impossible to estimate the fulcum point location $\{F''\}$ by (3) and (4) using $\overrightarrow{F_{H'}}$. For this reason, it is needed to know when this situation happens. This section proposes a solution for detecting interaction with tissue using both manipulators which is useful in order to estimate the fulcrum point location. For this purpose, three cases may be taken into account which are represented by Fig. 3. First case (a) represents both instruments without interaction with tissue

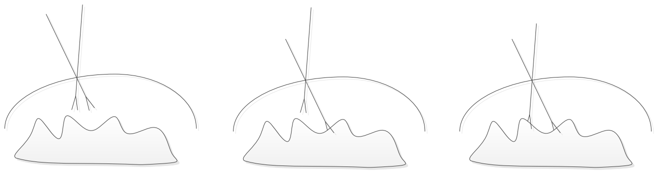

(a) (b) (c)

Fig. 3. Tissue interaction using two instruments.

($|\overrightarrow{F_P}| \approx 0$). In this case, a fusion sensor algorithm may be used in order to get more accuracy in the estimation, explained in next section. When only one instrument is interacting with tissue (b), only one F/T sensor may be used for it. At last, when both instruments are interacting with tissue, fulcrum point cannot be estimated and previous estimation should be used.

In order to detect if there is interaction with tissue, as stated above, a Hidden Markov Model (HMM) based algorithm is proposed. It is composed by a set of states S and observations e. On the other hand, it is necessary to define the state transition distribution matrix A, the observation symbol probability distribution matrix for each state B, and the initial state distribution π [18]. This information can be represented using the compact notation $\lambda = (A, B, \pi)$.

In this case, a circular HMM has been used [17]. This structure is shown in Fig. 4. Their states provide information about if the tip of the instrument is interacting with tissue or not and it is based on the observation sequence. For this purpose, four states $S = \{S_1, S_2, S_3, S_4\}$ and eleven observations $e = \{e_1, e_2, \dots, e_{11}\}$ have been defined.

Table I shows states which are represented in Fig. 4. States S_1, S_2 and S_4 denote a situation when there is no interaction with tissue ($Ti = 0$). State S_2 and S_4 are transition states. They have been defined in order to increase the number of states and therefore improve the HMM results.

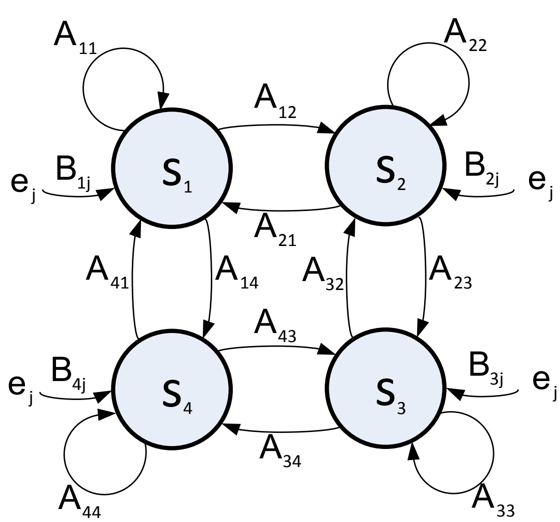

Fig. 4. Circular HMM for 4 states.

TABLE I. HMM STATES

States	Description	
	Abbrev.	*Description*
S_1	NT	Not touching tissue
S_2	NTT	Near to touch tissue
S_3	TT	Touching tissue
S_4	NNTT	Near to not touch tissue

On the other hand, set of defined observations V is represented in Table II. In this case, each observation represents a union of the movement carried out by a manipulator and forces read by the F/T sensor attached to this manipulator. A vertical movement is defined as a movement of the tip outside or inside, and a horizontal movement is defined as a movement in a perpendicular plane to the orientation of the tip. Also, F_h represents the module of forces on the F/T sensor horizontal plane and F_v represents the vertical forces. Also, F_t represents the module of all the exerted forces.

TABLE II. HMM OBSERVATIONS

Obs.	Description	
	Abbrev.	*Description*
e_1	V	Vertical movement without force ($F_v < F_{min}$)
e_2	Vf+	Vertical movement with higher force ($F_v > F_{max}$)
e_3	Vf-	Vertical movement with lower force ($F_{min} > F_v > F_{max}$)
e_4	H	Horizontal movement without force ($F_h < F_{min}$)
e_5	Hf+	Horizontal movement with higher force ($F_h > F_{max}$)
e_6	Hf-	Horiz. movement with lower force ($F_{min} > F_h > F_{max}$)
e_7	Q	No movement without force ($F_t < F_{min}$)
e_8	Qf+	No movement with higher force ($F_t > F_{max}$)
e_9	Qf-	No movement with lower force ($F_{min} > F_t > F_{max}$)
e_{10}	O	Instrument tip opened
e_{11}	C	Instrument tip closed

Once defined states and observations, to complete the specification of a HMM, it is necessary to define λ. In the case of π, it is known because the initial state is always the first one. On the other hand, A and B can be estimated using a sequence of observations with known states which can be obtained observing movements of instruments during the surgery and training the HMM using the Baum-Welch method [18].

Finally, current status, which defines if there is interaction with tissue or not, is obtained as explained below. Starting with a sequence of n previous observations with the current observation $O = o_{k-n} \dots o_{k-1}\, o_k$, and the λ model stated above. The objective is to find a state sequence $Q = q_{k-n} \dots q_{k-1}\, q_k$ which is the highest likelihood $\delta_k(i)$ (optimal state sequence) associated with the given observation sequence (5).

$$\delta_k(i) = max\ P(q_{k-n} \dots q_k = i, o_{k-n} \dots o_k|\lambda) \qquad (5)$$

The Viterbi algorithm [18] provides a solution for this problem and q_k provides the current status of the tip of the instrument, if it is interacting with tissue or not. It is worth mentioning that this algorithm may be implemented for each manipulator in order to use it for improving the fulcrum point estimation.

IV. Control Scheme

Proposed control scheme is based on a parallel position-force control algorithm. This algorithm is able to move the instrument to a desired orientation $\{F'\}$, taking into account the estimated fulcrum point using the interaction with tissue detector stated above and a Kalman filter measurement fusion method which merge fulcrum point estimations obtained by both manipulators.

Fig. 5 represents the proposed control scheme. A trapezoidal trajectory generator provides different position reference every cycle time on each manipulator, configuring velocities and accelerations without saturate their joints actuators. In the case when there is no interaction with tissue $T_i = 0$, each manipulator receives this reference with the increment induced by the force feedback, and they perform the planned trajectory taking into account this force using a Fuzzy Gain Tuner as controller which improves the system response due to the hysteresis effect by the space between instruments and trocar [19]. In order to perform this movement correctly, the estimated distance between the end effector and fulcrum point $\left|\overrightarrow{{}^{H'}D_{F''}}\right|$ is needed. For this purpose, three cases stated in Fig. 3 are taken into account. In the case when there is no interaction with tissue (Fig. 3.a), a fusion of fulcrum point estimations provided by both manipulators improves this estimation and therefore reduces the exerted forces in the abdomen. For this purpose, a discrete Kalman filter measurement fusion method is used [20]. This method combines measurements in order to obtain an estimated final state based on the fused observations. In this case, the estimated fulcrum point coordinates for each manipulator are modeled by a discrete-time state-space model (6) and (7), where k represents the discrete-time index, $p_F^{B_0} = [x_F^{B_0} \quad y_F^{B_0} \quad z_F^{B_0}]^T$ is the state-vector which represents the space coordinates for the fused estimated fulcrum point, $[p_{F_1'}^{B_0} \quad p_{F_2'}^{B_0}]^T$ is the measurement vector which represent the space coordinates of the fulcrum point estimated by each manipulator, and at last, w_k and v_k are zero-mean white Gaussian noise with covariance matrices Q_k and R_k. As will be demonstrated in the experimental results, this algorithm improves the fulcrum point estimation accuracy and therefore reduces exerted forces in the abdomen.

$${p_F^{B_0}}_{k+1} = {p_F^{B_0}}_k + w_k \qquad (6)$$

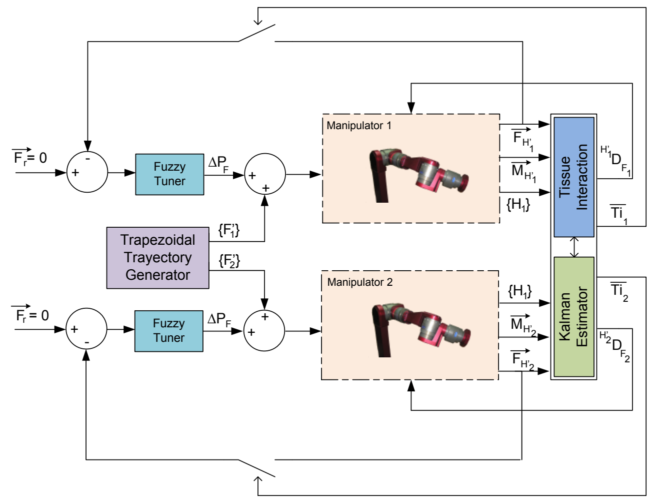

Fig. 5. Control scheme for two manipulators.

$$\begin{bmatrix} p_{F_1'}^{B_0} \\ p_{F_2'}^{B_0} \end{bmatrix}_k = \begin{bmatrix} 1 & 0 & 0 \\ 0 & 1 & 0 \\ 0 & 0 & 1 \\ 1 & 0 & 0 \\ 0 & 1 & 0 \\ 0 & 0 & 1 \end{bmatrix}_k \left[p_F^{B_0}\right]_k + v_k \qquad (7)$$

Position control for each manipulator (orange block in Fig. 5) is represented in Fig. 6. This scheme represents the orientation and position control for the reference orientation of the instrument at the fulcrum point $\{F'\}$ and the position increment ΔP_F. The difference between the sum of $\{F'\}$ and ΔP_F with the current orientation of $\{F''\}$ provides the cartesian and rotational velocities $\dot{P}$ and ω represented by $\dot{r} = (\dot{P}, \omega)$ in Fig. 6. Joint velocities $\dot{\theta}$ are obtained using the inverse Jacobian matrix. Also, the K_J gain is used in order to fix a dynamic for the manipulator which is approximated by a first-order system with time constant $1/K_J$ as demonstrate in [19]. Using an integrator, joint positions θ are achieved, and using the direct kinematic model, the new fulcrum point location $\{F''\}$ is calculated. Using the F/T sensor, the fulcrum point exerted force $\overrightarrow{F_{H'}}$ and torque $\overrightarrow{M_{H'}}$ are obtained.

V. Experiments

The aim of this section is to demonstrate experimentally how described algorithms work in a real environment: On the one hand, interaction with tissue detector and, on the other hand, the proposed control scheme using the Kalman filter based fusion sensor algorithm stated above. For this purpose, the CISOBOT platform has been used. This platform has been developed by the University of Malaga, and it is

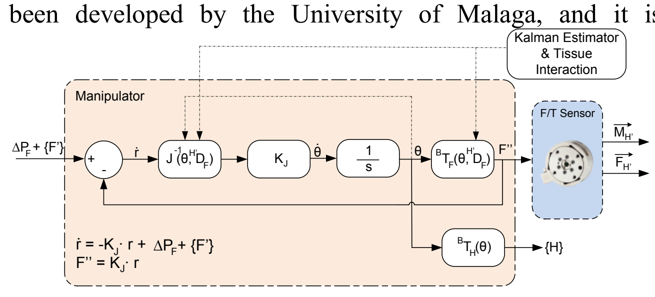

Fig. 6. Position control scheme for each manipulator.

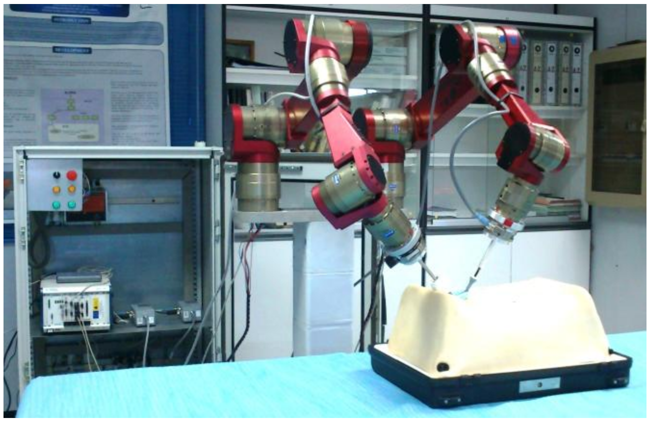

Fig. 7. Experimental scenario.

composed by two customized 6 DOF manipulators attached to a base with a weight compensation system. Also, F/T sensors have been placed between each end effector and experimental instruments. These instruments have been introduced through an abdomen simulator using a multiport trocar (Fig. 7).

A. Implementation

The CISOBOT platform is composed by six PRL Powercube system from Schunk Corp for each manipulator. This PRL has its own PID controller. Communications between it and the master controller are carried out using the standard CAN bus which provides a real-time interface. Moreover, this system performs movements using position or speed control. Based on the proposed control scheme, speed control has been used for performing movements.

Fig. 8 shows the implementation architecture which is described below. Matlab-Simulink environment with Real-Time Windows Target (SRTWT) has been used for both runtime and simulations. This software provides a real time environment for executing Simulink models on a Microsoft Windows Operative System. Due to the limited communications interface for SRTWT, another real time system, PXI from National Instruments, has been required. This system allows communications between SRTWT (limited to UDP protocol) and the PRLs (CAN Bus). Thus, a 15ms cycle time has been achieved.

Force sensors attached to manipulators are the Gamma 10 Netb SI-65-5 from ATI Automation. This sensor provides a UDP interface which enables it to connect directly to SRTWT. Also, it includes an internal noise filter and a gravity filter has been developed [21] which is needed for taking information only about the interaction with the abdomen and tissue.

B. Interaction with Tissue Experiment

Regarding to the interaction with tissue detector, a grasping action has been carried out in order to demonstrate how it works. In this case the manipulator performs a downward movement, it picks up tissue, and while it is moving upward tissue is released. Fig. 9 shows this experiment. First row represent position of the end effector in the Z axis, second row is the force read by F/T sensor, third and fourth rows represent detected observation based on

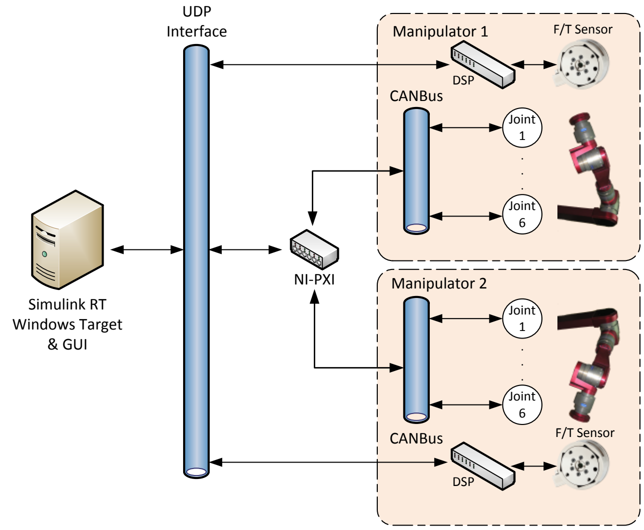

Fig. 8. Implementation architecture.

proposed HMM. For this experiment F_{min} and F_{max} has been fixed to 1N and 2N respectively.

Results of this experiments show when the manipulator is grasping tissue ($Time \approx 0.75\ sec.$), state three is activated, and when manipulator leaves tissue ($Time \approx 1.25\ sec.$), state changes to four and one. It does not match exactly with the instant when tissue is picked up and released, but this difference is not meaningful.

C. Control Scheme Experiment

For the case of the control scheme, stated experiment performs a movement which starts at location $\{H_1\}$=(532.1,-72.6,-307.2,2.2,2.142,-1.745) mm and radians, and $\{H_2\}$=(545.4,126.77,-277,-2.513,2.315,1.748). The fulcrum point location is $\{F\}$=(433,63.4,-415.3, 0, 0, 0) and there is no interaction with tissue. The performed movement is a $\pi/6$ rad rotation by the Y axis from the fulcrum point with duration of 1.5 seconds. This movement implies all the joints in order to evaluate the behavior of the manipulator described below. Fig. 7 represents the experimental scenario with both manipulators at the initial position. Each manipulator handles an instrument with different anchor, the instrument attached to the first manipulator has a diameter of 10mm and the second one has 5mm. The used multiport trocar is the *SILS Port* manufactured by Covidien.

Results of this experiment are shown in Fig. 10. In this figure, first and second rows show the abdominal exerted forces read by sensors $|\overrightarrow{F_{H_1}}|$ and $|\overrightarrow{F_{H_2}}|$ where oscillations are because of the space between instruments and trocar. The maximum peak level is 3.18N in manipulator 2, and the steady state measurement is lower than 1.5N. On the other hand, third and fourth rows represent the fulcrum point estimation error for each manipulator. At the end of simulation, this error is 6.3mm for manipulator 1 and 6.5mm for manipulator 2. It is worth mentioning that the Kalman Filter parameters have been tuned offline simulating the F/T sensors.

In order to compare obtained results, another three experiments have been carried out combining force feedback and Kalman filter estimation which are shown in TABLE III.

TABLE III. EXPERIMENTAL RESULTS

Exp.	Description				
	Force Feedback	***Kalman Estimation***	***Peak Force***	***Steady State Force***	***Steady State Est. Error***
1	Disabled	Disabled	6.5N	>6.5N	35mm
2	Disabled	Enabled	4.84N	>4.84N	21.6mm
3	Enabled	Disabled	3.87N	1.5N	36mm
4	Enabled	Enabled	3.18N	1.5N	**6.5mm**

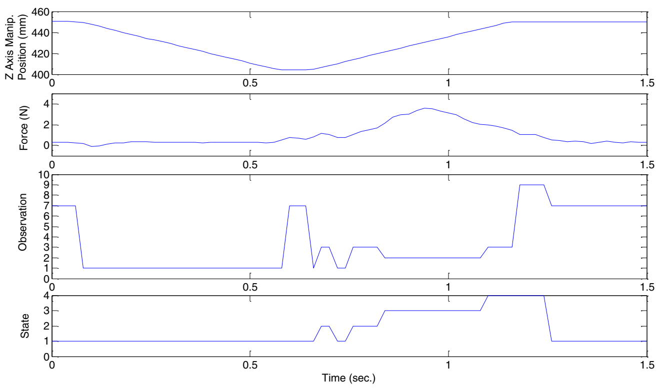

Fig. 9 Interaction with tissue detector experiment.

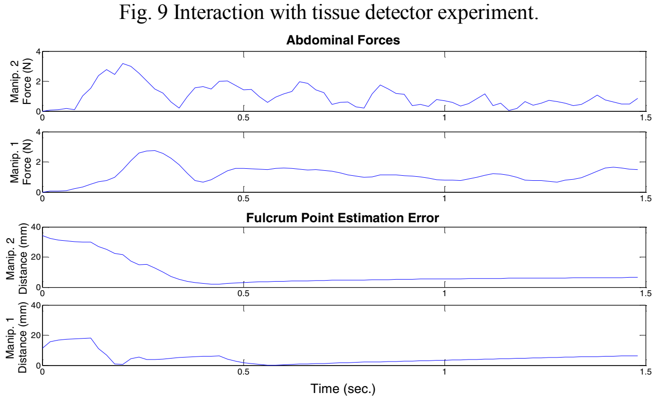

Fig. 10 Control scheme experiment.

VI. CONCLUSION

Results of this paper allow handling surgical instrument by two manipulators for SPAS using a multiport trocar. The main advantage which provides this method is the ability to orientate the surgical device in the correct way avoiding undesirable forces in the abdomen and improving the fulcrum point estimation using a Kalman filter based algorithm. Also, a HMM based method for detecting interaction with tissue has been defined and a grasping experiment has been carried out. However, a comparative between different HMM types and its experimental results with different actions (grasping, pushing, etc.) should be carried out. Furthermore, it is necessary to use instruments with distal joints in order to research about tissue interaction with these types of instruments. Finally, a haptic surgeon interface may be developed in order to teleoperate these manipulators and provide force feedback to the surgeon. These issues are proposed as future work.

REFERENCES

[1] Wedmid, A., Llukani, E. and Lee, D. I., “Future perspectives in robotic surgery”, *BJU International*, vol. 108, pp. 1028–1036, 2011.

[2] Paula Gomes, “Surgical robotics: Reviewing the past, analysing the present, imagining the future”, *Robotics and Computer-Integrated Manufacturing*, vol. 27, pp 261-266, Apr 2011.

[3] I. Halim, A. Tavakkolizadeh, "NOTES: The next surgical revolution?", *International Journal of Surgery*, vol. 6, pp. 273-276, August 2008.

[4] K. Kahnamoui, M. Cadeddu, F. Farrokhyar, M. Anvari, “Laparoscopic surgery for colon cancer: a systematic review” *Canadian Journal of Surgery*, vol. 50, pp. 48-57, Feb. 2007.

[5] N. Shussman, A. Schlager, et al. “Single-incision laparoscopic cholecystectomy: lesson learned for success”, *Surgical Endoscopy*, vol. 25, pp. 404-407, 2011.

[6] J. Shang, D.P. Noonan, et al. “An Articulated Universal Joint Based Flexible Access Robot for Minimally Invasive Surgery”, *IEEE International Conference on Robotics and Automation*, pp. 1147-1152, 2011.

[7] Jianzhong Shang, Christopher J. Payne, et al. “Design of a Multitasking Robotic Platform with Flexible Arms and Articulated Head for Minimally Invasive Surgery” *IEEE/RSJ International Conference on Intelligent Robots and Systems*, pp. 1988-1993, 2012.

[8] Marco Piccigallo, Umberto Scarfogliero, et al. “Design of a Novel Bimanual Robotic System for Single-Port Laparoscopy*” IEEE/ASME Transactions on Mechatronics*, vol. 15, no. 6, pp. 871-878, 2010.

[9] U. Hagn, R. K, onietschke, A. Tobergte, et al. “DLR MiroSurge: a versatile system for research in endoscopic telesurgery*”, International Journal of Computer Assisted Radiology and Surgery*, vol. 5, pp. 183-193, 2010.

[10] C. Freschi, V. Ferrari, F. Melfi, et al. “Technical review of the da Vinci surgical telemanipulator”, *The International Journal of Medical Robotics and Computer Assisted Surgery*, vol. 9, pp. 396-406, 2013.

[11] Chin-Hsing Kuo, J. S. Dai, P. Dasgupta, “Kinematic design considerations for minimally invasive surgical robots: an overview”, *The International Journal of Medical Robotics and Computer Assited Surgery*, vol. 8, pp. 127-145, 2012.

[12] M. Michelin, P. Poignet, E. Dombre, “Dynamic Task/Posture Decoupling for Minimally Invasive Surgery Motions: Simulation Results”, *IEEE International Conference on Intelligent Robots and Systems*, pp. 3625-3630, 2004.

[13] A. Krupa, G. Morel, M. Mathelin, “Achieving high-precision laparoscopic manipulation through adaptive force control”, *Advanced Robotics*, vol. 18, no. 9, pp. 905-926, 2004.

[14] Y. Kobayashi, P. Moreira, C. Liu, et al. “Haptic feedback control in medical robots through fractional viscoelastic tissue model”, *Enginerring in Medicine and Biology Society, EMBC, Annual International Conference of the IEEE*, pp. 6704-6708, 2011.

[15] E. Ruiz Morales, S. C. Correcher, “Force estimation for a minimally invasive robotic surgery system”, European Patent, publication number: EP2491884 A1, 2012.

[16] P. Huang, L. Gu, J. Zhang, X. Yu, et al. “Virtual Surgery Deformable Modelling Employing GPU Based Computation”. *17th International Conference on Artificial Reality and Telexistence*. Aalborg University Esbjerg, Denmark, pp. 221-227, 2007.

[17] V. Kellokumpu, G. Zhao, M. Pietikäinen, “Recognition of human actions using texture descriptors”, *Machine Vision and Applications*, vol. 22, pp. 767-780, 2011.

[18] L.R. Rabiner, “A Tutorial on Hidden Markov Models and Selected Applications in Speech Recognition”, *Proceedings of the IEEE*, vol. 77, pp. 257-286, 1989.

[19] C.J. Perez-del-Pulgar, V.F. Muñoz, J.J. Velasco, et al., “Parallel force-position control scheme with fuzzy gain tuning for single port laparoscopic surgery”, *International Conference on Control, Automation and Systems*, pp. 101-106, 2013.

[20] Gan, Q.; Harris, C.J., "Comparison of two measurement fusion methods for Kalman-filter-based multisensor data fusion," *Aerospace and Electronic Systems, IEEE Transactions on*, vol.37, no.1, pp. 273-279, Jan 2001.

[21] E. Bassi, F. Benzi, et al. “Characterization of the Dynamical Model of a Force Sensor for Robot Manipulators”, *Robot Motion and Control*, *Lecture Notes in Control and Information Sciences*, Vol. 396, pp 243-253, Springer-Verlag, 2009.